Hindbrain V2a neurons impose rhythmic activity on motor neurons in an *in vitro* reticulospinal circuit

Adele V Bubnys[1], Hagar Kandel[1], Lee-Ming Kow[1], Donald W Pfaff[1], Inna Tabansky[1,2]

[1] Laboratory of Neurobiology and Behavior, The Rockefeller University, New York, NY 10065. [2]Feinstein Institute for Medical Research, Manhasset, New York, NY 11030.

Abstract:

The reticulospinal system is an evolutionarily conserved pathway among vertebrates that relays locomotor control signals from the hindbrain to the spinal cord. Recent studies have identified specific hindbrain cell types that participate in this circuit, including Chx10^{+} neurons of the medullary reticular formation, which project to the spinal cord and are active during periods of locomotion. To create a system in which reticulospinal neurons communicate with spinal motor effectors, we have constructed an *in vitro* model using two purified excitatory neuronal subtypes: HB9^{+} spinal motor neurons and Chx10^{+} hindbrain neurons. Cultured separately, these neurons exhibit cell type-specific patterns of activity; the Chx10^{+} cultures developed regular, synchronized bursts of activity that recruited neurons across the entire culture, whereas motor neuron activity consisted of an irregular pattern. A combination of the two subtypes produced cultures in which Chx10^{+} neurons recruited the motor neurons into synchronized network bursts, which were dependent on AMPA receptors. In addition to demonstrating that the activity of *in vitro* networks can depend on the developmental identity of their constituent neurons, we provide a new model with genetically specified nerve cell types to study the activity of a reticulospinal circuit.

26   **Significance statement:**

27   Models of the brain that use cultured neurons are usually comprised of a complex

28   mixture of different kinds of cells, making it hard to determine how each cell type contributes

29   to the overall pattern of activity. We made a simplified culture containing two cell types known

30   to form a reticulospinal circuit *in vivo*. While in isolated cultures, each cell type had a distinct

31   pattern of activity, in coculture the activity of one cell type came to dominate, indicating that

32   the patterns observed in complex neuronal cultures arise in part from the distinctive properties

33   of the constituent neurons.

34   **Introduction:**

35   To derive clinically relevant findings, most *in vitro* models of neurological disease seek to

36   incorporate as realistic a mixture of cells from the modeled region as possible. These models of

37   disease hold therapeutic promise, as some have already been used to identify small molecule

38   candidates for drug development (Yang 2013, Wainger 2015, Ahfeldt 2017). Models of CNS

39   regions have also been shown to develop complex patterns of activity similar to their *in vivo*

40   counterparts (Trujillo 2018). Primary tissue taken from different areas of the brain and cultured

41   on multi-electrode arrays (MEAs) develops regular bursts of spiking activity with tissue-specific

42   differences in the shape of spike waveforms and the timing and structure of bursts (Dauth

43   2017, Soscia 2017, Sarkar 2018). When the different tissue types were co-cultured on a single

44   array they developed correlated activity, suggesting that they could communicate with each

45   other.

46   However, it is unclear whether these observations of bursts and changes in activity are

47   an emergent property of the mixture of cell types in these cultures or governed by the presence

48   of specific neuronal cell types (Maheswaranathan 2012, Chiappalone 2016, Lonardoni 2017). To

49   appreciate how network activity emerges in such cultures and how it is determined by the

50   properties of individual neuronal cell types, it is important to study each cell type in isolation

51   prior to combining them into a more complex system.

52   To address this question, we created a simple system from two neuronal subtypes with

53   a well-defined relationship in the intact nervous system, motor neurons and reticulospinal

54   neurons. Motor neurons relay patterned input from spinal cord central pattern generator

55   circuits to skeletal muscles to initiate behavior (Binder 1996). Reticulospinal neurons are

56   components of a prominent behavioral circuit that relays rhythmic locomotor drive from the

57   brainstem to the spinal cord (Peterson 1979, Garcia-Rill 1987a,b , Le Ray 2011, Kiehn 2016).

58   Of the subtypes of reticulospinal neurons, we specifically focused on V2a excitatory

59   interneurons, identified by expression of the transcription factor Ceh-10 Homeodomain-

60   Containing Homolog (Chx10, also known as Visual System Homeobox 2, or Vsx2), which are

61   found in the spinal cord and medullary reticular formation. Chx10$^+$ V2a neurons within the

62   hindbrain reticular formation play a role in regulating hindlimb locomotion (Bretzner 2013,

63   Bouvier 2015) and respiratory rhythm (Crone 2009, Crone 2012) and have functional

64   connectivity to the mesencephalic locomotor region and pre-Bötzinger complex.

65   We hypothesized that the reticulospinal neurons cultured on MEAs would develop a

66   different pattern of activity than motor neurons, which would be consistent with each subtype

67   having a distinct behavioral role. Because motor neurons are controlled by reticulospinal

68   neurons *in vivo*, we further hypothesized that the reticulospinal neurons' activity would come

69   to dominate in a combined coculture. This would support the idea that the electrical and

3

70   biochemical properties of one neuronal subtype can drive the activity of the entire network *in*

71   *vitro*.

72   Here, we report that Chx10+ hindbrain neurons develop synchronized network bursts

73   that differ from the uncorrelated and irregular activity of motor neurons, and that in coculture

74   motor neurons are recruited into Chx10+ neuron bursts. We then further identify some synaptic

75   mechanisms that drive these circuit dynamics.

76   **Methods:**

77   *Cell culture*

78   All cells were cultured at 37°C in 5% carbon dioxide and 95-100% humidity in Revco

79   Ultima II CO_2 incubators (Thermo Electron). Primary cortical glia were dissected and dissociated

80   from Swiss Webster mice at P1-4 using the protocol described in Schlidge *et al*. (2013). Mouse

81   pups were anesthetized with 5% isoflurane for five minutes, then decapitated. The forebrain

82   was separated from the cerebellum and midbrain. The corpus callosum was severed, then the

83   meningeal covering was peeled away. Forebrain tissue was dissociated in 10% trypsin (0.25%

84   EDTA, Gibco, 25200-056) and passed through a 35μm filter (Corning, 352235). Cells were

85   cultured on 100mm cell culture dishes treated with 0.1% gelatin (ATCC, PCS-999-027) at a

86   density of ~$5x10^4$ cells/cm^2 and grown until confluent, usually within 8 days. Glial culture media

87   contained high glucose DMEM (Sigma-Aldrich, 51441C), 10% heat inactivated fetal bovine

88   serum (ATCC, SCRR-30-2020), and 1% penicillin/streptomycin/antimycotic (Sigma-Aldrich,

89   A5955). Once the glia reached confluence, they were dissociated with trypsin and cultured on

90   sterile 5mm n.1 glass coverslips (Warner, 640700) treated with 1mg/ml Poly-D-Lysine

91   (Millipore, A-003-E) and 1mg/ml laminin (Corning, 354232) in 24-well plates at a density of

4

92   5×10^5 cells/well. Neurons were seeded on this feeder layer of glia once it reached confluence,

93   after about 8 days.

94   ES-cell derived motor neurons were generated using the protocol described in Wichterle

95   *et al*. (2002) from the HBG3 ES cell line, in which the enhanced green fluorescent protein (eGFP)

96   is expressed under the control of the HB9 promoter (courtesy of Wichterle lab). ES cells were

97   grown in ADFNK media that consisted of 1:1 DMEM/F12 (Millipore, DF-041-B): Neurobasal

98   (Gibco, 21103049), 10% knock out serum replacement (Gibco, 10828010), 1%

99   penicillin/streptomycin/antimycotic, and 1% GlutaMax supplement (Gibco, 35050061) for 2

100   days until they formed embryoid bodies. Media were supplemented on days 2 and 5 with $1\mu M$

101   retinoic acid (Sigma-Aldrich, R2625) and $1\mu M$ smoothened agonist (Calbiochem, 566661). On

102   day 6, embryoid bodies were dissociated with papain according to manufacturer's instructions

103   (Worthington, LK003150).

104   Unsorted HB9$^+$ motor neurons were plated on 5mm glass coverslips in a 24-well plate on

105   top of a feeder layer of glia at a density of 1×10^6 cells/well. HB9$^+$ neurons that underwent FACS

106   sorting were plated on Poly-D-lysine and laminin coated 5mm glass coverslips at a density of

107   5×10^5 cells/well. For glial coculture, sorted HB9$^+$ neurons were seeded on glass coverslips with a

108   feeder layer of astroctyes at a density of 5×10^5 cells/well. For multi-electrode recordings,

109   standard 60-elecrode multi-electrode arrays (MultiChannel Systems, 890276) were sterilized

110   and then coated with poly-D-lysine and laminin and seeded with 1×10^6 sorted HB9$^+$ neurons.

111   For glial coculture on multi-electrode arrays, poly-D-lysine and laminin treated arrays were

112   seeded with 5×10^5 glial cells that were grown to confluence prior to seeding with 1×10^6 sorted

113   HB9$^+$ neurons. Media consisted of the BrainPhys neuronal medium (StemCell, 5792)

114   supplemented with 2% NeuroCult SM1 neuronal supplement (StemCell, 5711), 1% N2-

115   supplement (Gibco, 17502048), 1% GlutaMax supplement, 1% pen/strep/antimycotic, 1μM

116   Adenosine 3',5'-cyclic monophosphate, N^6,O2'-dibutyryl-sodium salt (dbCaMP, Calbiochem,

117   28745), 10ng/ml Brain derived neurotrophic factor (BDNF, MACS, 130-093-811), 10ng/ml Glial

118   derived neurotrophic factor (GDNF, GoldBio, 1170-14-10), and 1μM ascorbic acid (Sigma-

119   Aldrich, A4403). To produce HB9::GFP negative control for FACS sorting, ES-cell derived HB9$^+$

120   motor neurons were generated in parallel from the E14 ES cell line (courtesy of Hatten lab).

121   Reticulospinal Chx10$^+$ neurons were dissected from E12.5 mouse embryonic hindbrains

122   using the protocol described in Fantin *et al.* (2013) from mice in which the cyan fluorescent

123   protein (CFP) is expressed under the control of the Chx10 promoter (Zhong *et al*, 2010). To

124   produce the cells, a male mouse homozygous for Chx10::CFP (courtesy of Sharma lab) was

125   mated with a Swiss Webster female mouse (Taconic). On day E12.5 of the pregnancy, the

126   pregnant female was anesthetized in 5% isofluorane and oxygen and euthanized via cervical

127   dislocation.

128   For the hindbrain dissection, each embryo was decapitated just rostral to the forelimb

129   and the neural tube was isolated from the rest of the tissue. The developing rhombencephalon

130   (hindbrain) segment corresponding to the position of the reticular formation in adults was

131   excised and trimmed at the rostral and caudal ends. Dissections were performed in ice cold

132   HBSS buffer (Gibco, 14175-095) supplemented with 1% pen/step/antimycotic, 20mM D-glucose

133   (Sigma-Aldrich, G8769), and 1μM ascorbic acid. Hindbrains were dissociated with papain and

134   sorted using flow cytometry to isolate the Chx10$^+$ subpopulation. To produce Chx10::CFP

135   negative control for FACS sorting, E12.5 hindbrains were derived from Swiss Webster mouse

6

136   embryos. Sorted Chx10$^+$ hindbrain neurons were seeded on either 5mm glass coverslips in a 24-

137   well plate or multi-electrode arrays, both prepared with a confluent layer of glia, at a density of

138   1x10^4 neurons/well of coverslips or 4x10^4 neurons/array. All Chx10$^+$ hindbrain neurons were

139   cultured in Neurobasal medium supplemented with 2% SB-27 (Gibco, 17504044), 1% GlutaMax,

140   1% pen/strep/antimycotic, 1μM dbCaMP, 10ng/ml BDNF, 10ng/ml GDNF, and 1μM ascorbic

141   acid.

142   For reticulospinal cocultures, sorted HB9::GFP$^+$ motor neurons and Chx10::CFP$^+$

143   hindbrain neurons were seeded together on a confluent layer of glia on either 5mm coverslips

144   or multi-electrode arrays. On coverslips in a 24-well plate, HB9$^+$ neurons were seeded at a

145   density of 2.5x10^5 cells/well and Chx10$^+$ neurons were seeded at a density of 1x10^5 cells/well.

146   On multi-electrode arrays, HB9$^+$ neurons were seeded at a density of 1x10^6 cells/dish and

147   Chx10$^+$ neurons were seeded at a density of 4x10^5 cells/dish. Cocultures were grown in the

148   same supplemented BrainPhys medium used for HB9$^+$ cultures.

149   *Animals*

150   Mice were group housed in a 12-hour light/dark schedule, with food and water provided

151   *ad libitum*. For timed matings, two females were introduced into the home cage of a single

152   male, where they remained for the duration of the mating. Females were checked for vaginal

153   plugs every 24 hours and removed to separate cages after plug was detected, and singly housed

154   for the duration of the timed pregnancy. All animal procedures and protocols were approved by

155   the Rockefeller Institutional Animal Care and Use Committee.

156

157

7

158   *Flow Cytometry*

159   All samples were sorted on the basis of fluorescent marker expression on the BD

160   FACSAriaII benchtop flow cytometer with a 100μm nozzle and 20psi sheath pressure. Flow

161   cytometry was performed at the Flow Cytometry Resource Center at Rockefeller University.

162   To isolate HB9::GFP$^+$ motor neurons, embryoid bodies derived from HBG3 ES cells were

163   dissociated on day 6 using papain and resuspended in FACS buffer for embryoid bodies that

164   contains phenol-free HBSS supplemented with 2% heat-inhibited horse serum (Gibco,

165   26050088) and 5U/mL DNAse (Worthington, LK003172). For the GFP negative control,

166   embryoid bodies were derived from E14 ES cells and prepared under parallel conditions.

167   Between 10 and 20nM DAPI (Invitrogen, D1306) was added to each sample as a dead-cell

168   exclusion dye. Each sample was excited by a violet 405nm laser and dead cells were excluded

169   on the basis of emission in the DAPI wavelength 461nm using the 405D filter. Single cells were

170   distinguished from doublets on the basis of forward and side scatter of the sample comparing

171   the scatter area versus width. GFP fluorescence was detected using illumination from a 488nm

172   blue laser equipped with a 535/30nm filter and the gate for GFP$^+$ cell isolation was set based on

173   a comparison of the GFP fluorescence of the HBG3-derived sample and the E14-derived sample.

174   Typically, 50-60% of input cells from HBG3-derived embryoid bodies expressed GFP.

175   For Chx10::CFP$^+$ hindbrain neurons, hindbrains from Chx10::CFP$^{+/-}$ mice were dissociated

176   at E12.5 using papain and resuspended in FACS buffer for hindbrains that contains high glucose

177   phenol-free DMEM supplemented with 10% heat-inactivated fetal bovine serum, 1%

178   pen/strep/antimycotic, and 5U/ml DNAse. For the CFP-negative control, hindbrains from Swiss

179   Webster mice were prepared under parallel conditions. Approximately 20nM ToPro3

180   (Invitrogen, T3605) was added to each sample as a dead cell exclusion dye. Each sample was

181   excited by a red 640nm laser, dead cells were excluded on the basis of emission in the ToPro3

182   wavelength using the 640C 670/30nm filter. As with the HB9::GFP$^+$ motor neurons, single cells

183   were distinguished from doublets on the basis of forward and side scatter area versus width.

184   CFP fluorescence was detected using illumination from a 445nm blue violet laser equipped with

185   a 490/30nm filter and the gate for CFP$^+$ cell isolation was set based on a comparison of the CFP

186   fluorescence of the Chx10::CFP$^{+/-}$-derived sample and the Swiss Webster-derived sample.

187   Typically, 2.5-3% of input cells from Chx10::CFP$^{+/-}$ mouse hindbrains expressed CFP.

188   *Electrophysiology*

189   Coverslips containing neurons cultured on a feeder layer of astrocytes as described

190   above (see Cell Culture methods) for 5 to 10 days were perfused with 1x HEPES-ACSF in the

191   recording chamber (HEPES-ACSF: 135mM NaCl, 10mM HEPES, 10mM glucose, 5mM KCl, 1mM

192     $CaCl_2$-$2H_2O$, 1mM $MgCl_2$) under constant flow (~5ml/minute). All cells were patched using

193   pulled glass pipettes with an R_E of 5 to 12 MΩ filled with a standard internal pipette solution (K-

194   gluconate: 14mM, HEPES-K: 10mM, $NaHCO_3$: 60μM, Mg-ATP: 4mM, Na_2-ATP: 2mM, Na-GTP: 30

195   μM, sucrose: 8mM, $CaCl_2$: 1mM, EGTA: 5μM). Data were acquired on the MultiClamp 700B

196   (Axon instruments) using ClampEx software. HB9$^+$ spinal motor neurons were identified by GFP

197   signal imaged using an Olympus BXS1W1 upright fluorescence microscope equipped with a

198   FITC/EGFP filter (480/535nm ex/em, Chroma). Chx10$^+$ hindbrain neurons were identified by CFP

199   signal from an ECFP filter (436/480nm ex/em, Chroma).

200   Once a giga-seal was achieved, the membrane voltage of the neuron was recorded for 1

201   minute at 1kHz sampling frequency without injecting additional current to measure the

202   spontaneous activity of the neuron. For current-clamp experiments, current was injected to

203   bring V_m to -70mV and current steps were applied in 10pA increments from -10 to 130pA for 1

204   second duration, returning to -70mV holding potential between steps. For voltage clamp

205   experiments, the cell was held at -80pA for 100ms before stepping voltage injection from -100

206   to 150mV in 10mV increments for 100ms, returning to the -80pA holding potential between

207   each step.

208   Data analysis and plotting of patch clamp data were performed using ClampFit and

209   Matlab (see github.com/abubnys/patch_clamp_analysis for specific scripts used). To generate

210   IV plots of voltage-gated sodium current from voltage-clamp data, the local minimum evoked

211   current within 30ms of voltage step onset was subtracted from the mean current during the

212   last 30ms of the voltage step and plotted against the magnitude of the injected voltage.

213   *Multi-electrode recordings*

214   Multi-electrode arrays were cultured with HB9^{+} motor neurons or Chx10^{+} hindbrain

215   neurons as described above (see Cell Culture methods). For the duration of the lifetime of the

216   culture (D3 to D30 days after plating for Chx10^{+} and D7 to D30 days after plating for HB9^{+}

217   neurons), spontaneous extracellular activity was recorded using the MEA2100-Lite system

218   (MultiChannel Systems). The array was placed in the recording apparatus and allowed to

219   equilibrate at room temperature for 30 minutes prior to recording for 4 minutes. Data

220   acquisition was performed on MCRack with an input voltage range of -19.5 to +19.5mV and a

221   sampling frequency of 20kHz. Raw electrode data for 60 electrodes were processed through a

222   Bessel 4th order high pass filter with a cutoff at 400Hz. The spike detection threshold was 5

223   standard deviations below the mean of the filtered recordings. Raw and filtered data, along

224   with spike timestamps were converted to .txt files using MC_DataTool and the resulting files

225   were analyzed in Matlab.

226   For wash-in experiments of the synaptic blockers 6-cyano-7-nitroquinoxaline-2,3-dione

227   disodium salt (CNQX), D-(-)-2-amino-5-phosphonopentanoic acid (AP5), and bicuculline on the

228   multi-electrode arrays, warmed 1x HEPES-ACSF was perfused through the MEA after the 30-

229   minute equilibration period at ~5ml/minute for 10 minutes. The baseline activity of the MEA

230   was recorded for 2 minutes under the previously mentioned parameters. Then, 100uL of a 10x

231   solution of the drug was slowly perfused in at 50μL/minute for 2 minutes while recording. After

232   2 minutes the pump was stopped and the steady-state activity of the array in the presence of

233   the drug was recorded for 4 minutes. The MEA was washed with 1x HEPES-ACSF at 5ml/minute

234   for 10 minutes in between drug applications. Filtered electrode data were converted using

235   MC_DataTool and analyzed in Matlab. The final concentrations of the drugs used were 20μM

236   CNQX (Tocris, 479347-85-8), 50μM AP5 (Tocris, 79055-68-8), and 60μM bicuculline (Tocris,

237   UN1544).

238   Data analysis for perfusion experiments was performed in Matlab (see

239   github.com/abubnys/MEA_perfusion_package for specific scripts used). For initial spike data

240   extraction, the high-pass filtered recordings from each electrode generated by MC_Rack

241   (multichannel systems, Reutlingen, Germany) were converted into .txt format using

242   MC_DataTool (multichannel systems). Spikes were detected in each channel using a manual

243   threshold adjusted to pick up deviations that were approximately five standard deviations

244   below the baseline of the recording and analysis of spike waveforms was used to determine

245   whether one or more neurons was contributing to the observed signal. Spike sorting was

246   performed on these data by plotting the aggregate collection of waveforms from recorded

247   spikes. If this collection of waveforms fell within multiple visually distinguishable distributions,

248   manual thresholds for each distribution were set by drawing a line through the waveforms

249   visually classified as similar and then categorizing all recorded spikes according to whether they

250   cross this threshold line or not. Then, spike rate was calculated for each waveform type by

251   counting the number of spikes that fall within bins of 100ms width and multiplying by 10 to

252   covert to units of Hz.

253   To facilitate comparison of different spike rates across all recordings, spike rates were

254   smoothed using a spline function, binned according to the average spike rate in non-

255   overlapping 10s intervals, then normalized to set the average spike rate from the first 10 bins

256   (corresponding to the first 100s of recording) to 1.

257   To determine whether synaptic blocker wash-in had a dose-dependent effect on the

258   activity of each culture type, normalized spike rate data from each electrode on the MEA that

259   recorded spontaneous neuronal activity were pooled across all drug wash-in trials for a given

260   culture type. The data corresponding to the period when the drug was washed in (2-4 minutes

261   into the recording) were fit to a linear mixed effects model using the function fitlme() in Matlab

262   with the normalized spike rate as the predictor variable and electrode as the random effect:

263   Drug dose (μM) ~ 1 + normalized spike rate + (1|electrode)

264

265

266   *Calcium imaging*

267   HB9^{+}, Chx10^{+}, or combined cocultures grown on 5mm coverslips with a feeder layer of

268   glia were loaded with Rhod-3 AM dye according to the manufacturer's instructions (Molecular

269   Probes, R10145), then washed with 1x HEPES-ACSF. Calcium imaging was subsequently

270   performed in 1x HEPES-ACSF.

271   For Chx10^{+} cultures, calcium reporter dye fluorescence during spontaneous activity was

272   imaged using an inverted spinning disc confocal microscope (Zeiss Axiovert 200) equipped with

273   an EMCCD camera (Andor iXon). Solid state lasers were used for excitation at 443 and 561nm

274   (Spectral Applied) paired with a polychroic filter with 440nm, 491nm, 561nm, and 640nm

275   filters. Imaging acquisition was performed using MetaMorph software. Chx10^{+} neurons were

276   identified by CFP signal (440/480nm ex/em) and rhodamine3 signal was identified on the Texas

277   Red channel (561/620-60nm ex/em). Calcium imaging data were acquired via time-lapse, with a

278   150ms interval and 100ms exposure time for 2 minutes.

279   For HB9^{+} cultures, HB9/Chx10 cocultures, and astrocyte cultures, spontaneous calcium

280   activity was imaged at room temperature and ambient CO_2 using an Olympus BXS1W1 upright

281   fluorescence microscope equipped with an Evolution QEi digital CCD camera

282   (MediaCybernetics). A 120W mercury vapor short arc bulb was used as the fluorescence light

283   source (X-Cite series 120Q). Imaging acquisition was done using NIS-Elements BR software.

284   Hb9^{+} spinal motor neurons were identified by GFP signal using a FITC/EGFP filter (480/535nm

285   ex/em, Chroma) and imaged with an exposure time of 100ms.

13

286   Chx10$^+$ hindbrain neurons were identified by CFP signal using an ECFP filter (436/480nm

287   ex/em, Chroma) and imaged with an exposure time of 100ms. Rhodamine3 signal was imaged

288   using a CY3/TRITC filter (545/605nm ex/em, Chroma) with an exposure time of 60ms per frame

289   for 40 to 80 seconds.

290   For experiments involving application of the AMPA$_R$ blocker CNQX, the spontaneous

291   calcium activity of HB9/Chx10 cocultures in HEPES-ACSF solution was imaged to determine a

292   baseline level of activity. Then, 200µl of a 100x solution of CNQX was injected into the bath for

293   a final drug concentration of 40µM. The culture was allowed to equilibrate for five minutes

294   before imaging of spontaneous calcium activity in the presence of the drug. The drug was

295   washed out by replacing 50% of media with fresh HEPES-ACSF in 5 repeated washes, then the

296   culture was allowed to equilibrate for 5 minutes before measuring recovery of spontaneous

297   activity.

298   Calcium imaging data for all experiments were analyzed in Matlab (see

299   github.com/abubnys/calcium_imaging_ROI_analysis for specific scripts used). Due to overlap

300   between CFP and GFP emissions spectra, CFP$^+$ neurons appear on the GFP fluorescence channel

301   and were distinguished from HB9::GFP$^+$ neurons on the basis of their fluorescence on the CFP

302   channel. ROIs were manually drawn around the cell bodies of identified CFP$^+$ and GFP$^+$ neurons

303   and the mean Rhodamine3 fluorescence within the ROI was calculated at each frame of the

304   recording in the Rhod3 channel.

305   Editing of rhodamine3 fluorescence time-course videos was performed in Fiji. For each

306   video, brightness and contrast was adjusted uniformly across the image stack using the "auto"

307   adjust function. Then, the minimum intensity for each pixel across the image stack (calculated

14

308   using the "Z-project, minimum" function) was subtracted from each image in the stack to

309   remove noise. Then, brightness and contrast were adjusted again across the image stack. Video

310   playback is 20fps.

311   *Statistical Methods*

312   All statistical analyses were performed in Matlab. Results are presented as mean $\pm$ SEM.

313   For patch clamp experiments, age matched HB9::GFP$^+$ neurons from cultures that were either

314   immediately plated after dissociation from embryoid bodies or underwent flow cytometry prior

315   to plating were subjected to the same battery of current clamp, voltage clamp, and

316   spontaneous activity recordings. Student's t-test was used for between-group comparisons of

317   voltage-gated I_{Na} and spike threshold. For MEA recordings, cross-correlation was used to

318   determine the degree of coordination across electrodes that detected spontaneous activity

319   from each recording. For synaptic blocker experiments, all electrodes with spontaneous activity

320   from MEA recordings were pooled according to culture type and normalized. To determine if

321   there was a dose-dependent effect of synaptic blocker on spike rate, this data was fit to a linear

322   mixed effects model. The statistical significance level for all of these analyses was set to $p < 0.05$.

323   *Code accessibility*

324   All custom written code used for this study is available on github. The code used to

325   analyze and visualize patch clamp data is available at github.com/abubnys/

326   patch_clamp_analysis. Code for quantifying calcium imaging data is available at

327   github.com/abubnys/calcium_imaging_ROI_analysis. The code used for extracting and

328   analyzing data from synaptic blocker perfusion experiments on MEAs is available at

329   github.com/abubnys/ MEA_perfusion_package.

15

Results:

Developing reticulospinal cultures

Numerous studies of mixed populations of neurons from various brain regions including cortex, amygdala, and spinal cord have a strong tendency to develop network bursts when cultured on extracellular multi-electrode arrays. These bursts occur when many neurons across the cultured network fire at once at regular intervals (Wagenaar 2006, Black 2017, Dauth 2016, Van Pelt 2005). It is generally believed that the generation of such bursts requires a combination of excitatory and inhibitory interneurons that work in concert to balance network activity between a state of excitation and complete quiescence (Maheswaranathan 2012, Li 2009, Sternfeld 2017).

We sought to test this hypothesis by purifying neuronal subpopulations, which allowed us to culture identified neurons at defined stages of development. We focused specifically on reticulospinal cultures containing homogeneous populations of HB9^{+} spinal motor neurons and hindbrain Chx10^{+} neurons. Hindbrain Chx10^{+} neurons are known to play a role in regulating locomotor gait and breathing rhythm and they have descending projections to the spinal cord (Bretzner 2013, Bouvier 2015, Crone 2012). Spinal motor neurons provide direct limb muscle innervation. Thus, the *in vivo* function of both neuronal subtypes predisposes them to rhythmic bursts.

To isolate pure populations of HB9^{+} spinal motor neurons and hindbrain Chx10^{+} neurons, we employed fluorescence activated cell sorting (FACS). We cultured these cell types as single populations and also as a mixed reticulospinal culture. We differentiated HB9^{+} spinal motor neurons from HBG3 embryonic stem cells using Wichterle et al's protocol to induce the

16

352   spinal motor neuron identity (Wichterle 2002). Embryoid bodies were dissociated 6 days after

353   formation and sorted on the basis of HB9::GFP expression. E14 stem cells lacking GFP were

354   used as a negative control for FACS (**Figure 1b,c**). Approximately 50-60% of unsorted cells in the

355   embryoid body derived from HBG3 ES cells expressed GFP. FACS sorting for GFP expression

356   enriched this population to >96% purity. HB9::GFP$^+$ motor neurons were subsequently cultured

357   on a layer of cortical astrocytes to improve axonal outgrowth and network development.

358   To test whether sorting affected the electrophysiological activity of HB9$^+$ neurons, we

359   performed whole cell patch clamp on HB9::GFP$^+$ neurons from sorted and unsorted cultures

360   grown in parallel under identical conditions. After 7 days in culture, HB9$^+$ neurons in both

361   treatments responded to brief current pulses with spike trains, having a spike threshold around

362   20pA (**Figure 2a,b**). They developed voltage gated sodium current (I_{Na}) with maximum current

363   evoked at -2±12 mV (**Figure 2c-e**) that was not significantly different between sorted and

364   unsorted populations (Student's 2-tailed T-test p = 0.879). After 13 days in culture, both sorted

365   and unsorted HB9$^+$ motor neurons also developed spontaneous spike trains (**Figure 2f**).

366   We then isolated and cultured primary hindbrain neurons expressing the transcription

367   factor Chx10, also using the FACS approach. We first assessed the Chx10$^+$ neurons' behavior *in*

368   *vitro* as a homogeneous population, and then in combination with HB9$^+$neurons to determine if

369   they could form a reticulospinal circuit *in vitro*. For these experiments, we dissected neurons

370   from embryonic Chx10::CFP$^{+/-}$ mice at E12.5, prepared a single cell suspension and used FACS to

371   isolate the CFP$^+$ population. As a negative control for CFP expression, we used hindbrains taken

372   from wildtype (WT) Swiss Webster E12.5 mouse embryos that do not express CFP (**Figure 1d,e**).
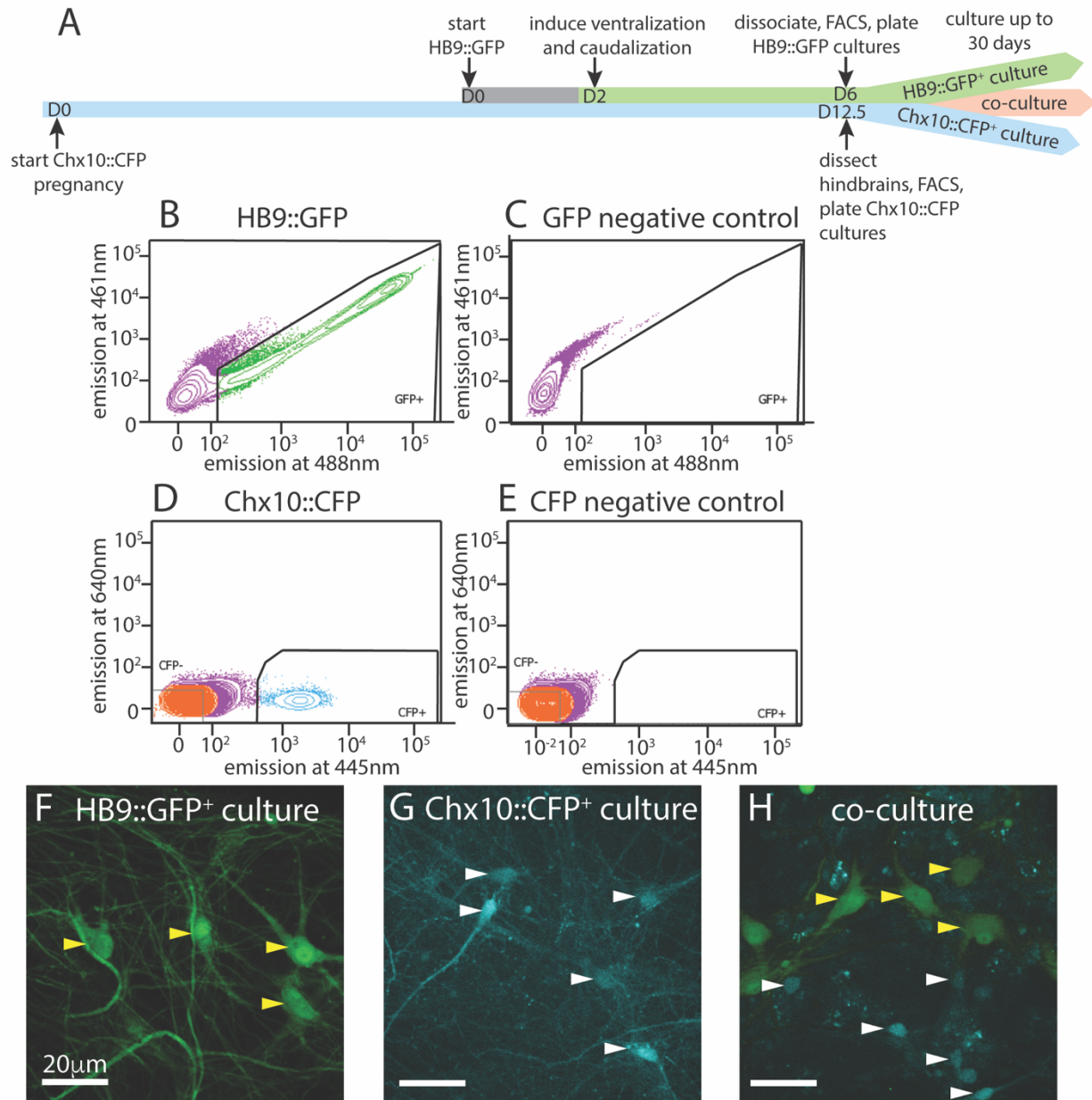
373

Figure 1: Isolation and culture of HB9+ motor neurons and Chx10+ hindbrain neurons. **A**, Timeline schematic of isolating and setting up HB9::GFP+, Chx10::CFP+, and combined co-cultures.
B-E Sample FACS plots and thresholds for isolation of Hb9::GFP+ and Chx10::CFP+ neurons. **B,** GFP+ neurons from HB9::GFP stem-cell derived embryoid bodies after 6 days in culture (DIC) **C,** embryoid bodies derived from non-transgenic ES cells (negative control) **D,** CFP+ neurons from E12.5 hindbrains of Chx10::CFP mice and **E,** Swiss Webster mice (negative control).
F-H Fluorescent photomicrographs of neurons cultured after sorting. Yellow arrowheads indicate HB9::GFP+ neurons and white arrowheads indicate Chx10::CFP+ neurons. **F**, Sorted HB9::GFP+ neurons, 16 DIC. **G**, sorted Chx10::CFP+ hindbrain neurons, 10 DIC (scale bar 20μm) **H**, combined culture of both subtypes, 16 DIC (scale bar 20μm).

374

18

375   The hindbrains contained 2-3% Chx10::CFP$^+$ neurons, and sorting enriched this population to

376   >95% purity. These CFP$^+$ neurons were then cultured on a layer of cortical astrocytes, which is

377   known to improve the development and long-term viability of neuronal cultures (Wang 1994,

378   Maher 1999, Boehler 2004).

379   It is possible that, when removed from the intact reticular formation with its descending

380   inputs and diversity of other cell types, Chx10$^+$ hindbrain neurons would not develop any

381   intrinsic activity that could pattern a reticulospinal circuit. To assess the electrophysiological

382   development of sorted Chx10$^+$ neurons, we used whole-cell patch clamp to record the

383   spontaneous activity of single cells in cultures at different ages ranging from 1 to 30 days in

384   culture. For Chx10$^+$ hindbrain neurons, the measured membrane capacitance was 22.75$\pm$2pF,

385   membrane resistance was 787.27$\pm$105MΩ, access resistance was 29.01$\pm$3MΩ, and membrane

386   voltage was -22.6$\pm$4mV. We found that Chx10$^+$ hindbrain neurons developed spontaneous

387   electrophysiological activity after 5 days in culture. This activity started off as random trains of

388   spikes, but gradually became organized into robust, regular bursts by 10 days in culture and this

389   pattern of activity continued throughout the remaining lifetime of the cultures (**Figure 2g**).

390   *Motor and Chx10 neuron cultures develop distinct patterns of network activity*

391   Having established that HB9$^+$ motor neurons and Chx10$^+$ hindbrain neurons develop

392   spontaneous electrophysiological activity at the single cell level, we sought to determine

393   whether cultures of either cell type, which are composed almost exclusively of excitatory

394   neurons and astrocytes, could generate spontaneous patterns of network activity, whether

395   these patterns would organize into network bursts, and whether there were any cell-type

396   specific differences in such activity.
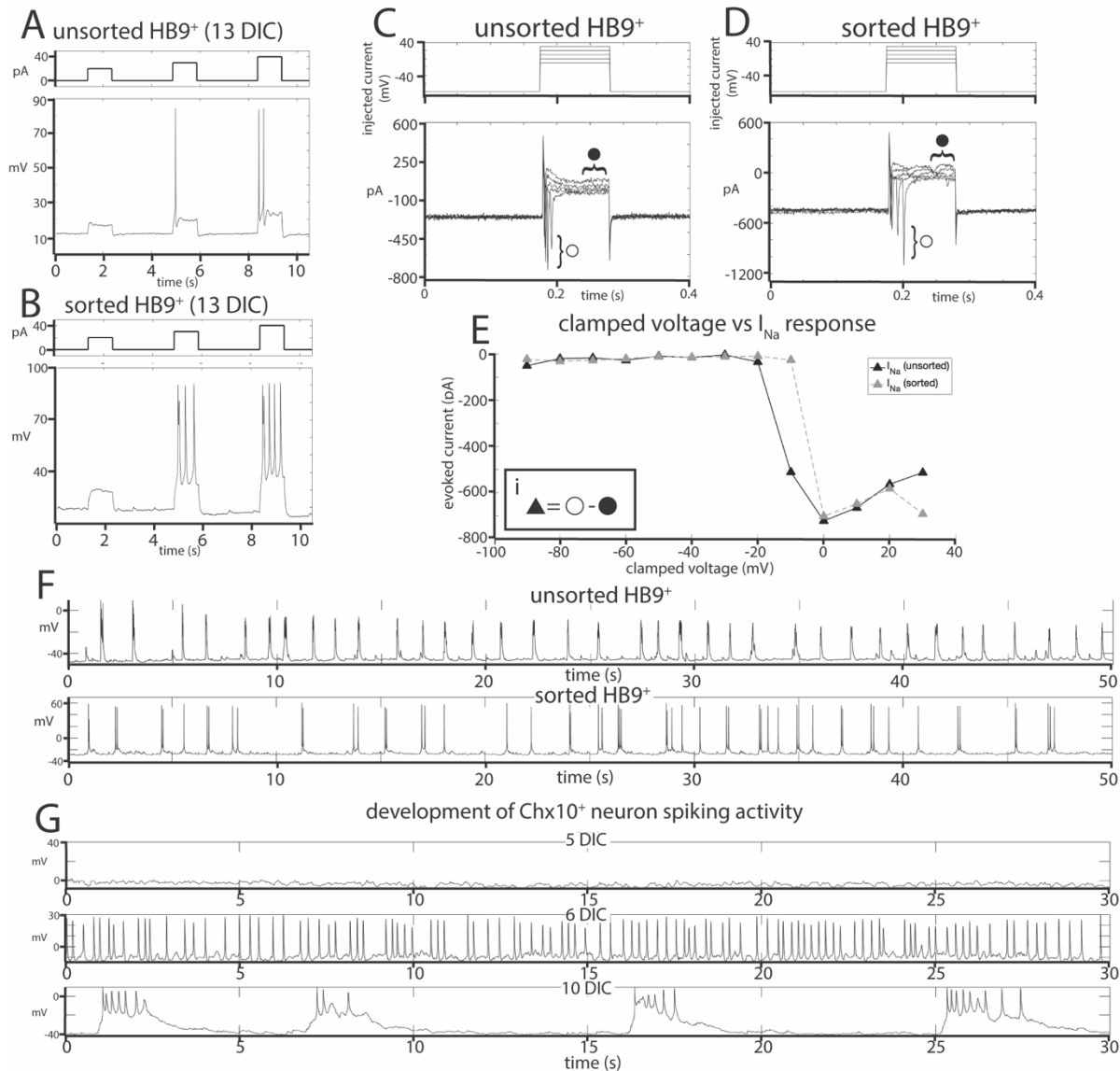
397

398

Figure 2: Effects of FACS sorting on neuron electrophysiology. **A-B** Comparison of the response of **A**, unsorted and **B**, sorted HB9::GFP⁺ neurons (bottom panels) to injections of 20, 30, and 40pA current (top panels).
C-D Response of **C**, unsorted and **D**, sorted HB9::GFP⁺ neurons (bottom panels) to voltage step injection of -90 to 30mV (top panels, result for -10 to 30mV injections shown) (7 DIC). Sodium current (I_{Na}) was calculated at each injected voltage step by subtracting the steady state current response (•) from the initial current minimum (o) (formula shown in insert *Ei*). **E**, I-V plot of Na⁺ currents for sorted and unsorted HB9::GFP⁺ neurons calculated from the voltage clamp experiment results shown in *C* and *D*. **F**, Spontaneous activity of unsorted (top panel) and sorted (bottom panel) HB9::GFP⁺ cells at 13 DIC**.** **G**, Spontaneous activity of sorted Chx10::CFP⁺ neurons at 5 DIC (top), 6 DIC (middle) and 10 DIC (bottom).

399   To record the activity of multiple neurons at different time points, we cultured sorted

400   HB9+ motor neurons on multielectrode arrays (MEAs) containing a grid of 64 extracellular

401   recording electrodes. We recorded their spontaneous activity daily over 30 days, starting from

402   the day after plating.

403   We found that on their own, without astrocytes, sorted HB9+ motor neurons did not

404   develop any spontaneous activity on the MEA (n = 6). However, when these neurons were

405   cultured on a confluent layer of astrocytes, they gradually developed robust network activity

406   that remained stable over a month of recording (n = 14). We note that astrocytes cultured on

407   their own did not develop spontaneous activity when recorded on MEAs (n = 3), although we

408   did observe spontaneous calcium flux in astrocyte cultures visualized with the calcium-sensitive

409   dye Rhodamine3 (**Video 3-1**). The activity of HB9+ motor neuron/astrocyte cultures was not

410   well coordinated, even among neighboring recording electrodes (**Figure 3a-c**). To assess

411   whether the overall activity of the culture had a hidden underlying temporal structure, we

412   calculated the mean spike rate across all active channels of the HB9+ motor neuron cultures and

413   found that it remained constant throughout the recording session (**Figure 3d**).

414   When we used the calcium-sensitive dye Rhodamine3 to assess HB9+ motor neuron

415   activity with single-cell resolution, we observed randomly distributed calcium spikes that were

416   asynchronous between neighboring neurons (**Figure 3e, Video 3-2**), though more mature

417   cultures did develop some synchrony (**Figure 3f, Video 3-3**). The mean correlation coefficient

418   between the spike rates of multiple neurons within the same HB9+ neuron culture was

419   0.15±0.17 (p = 0.15).
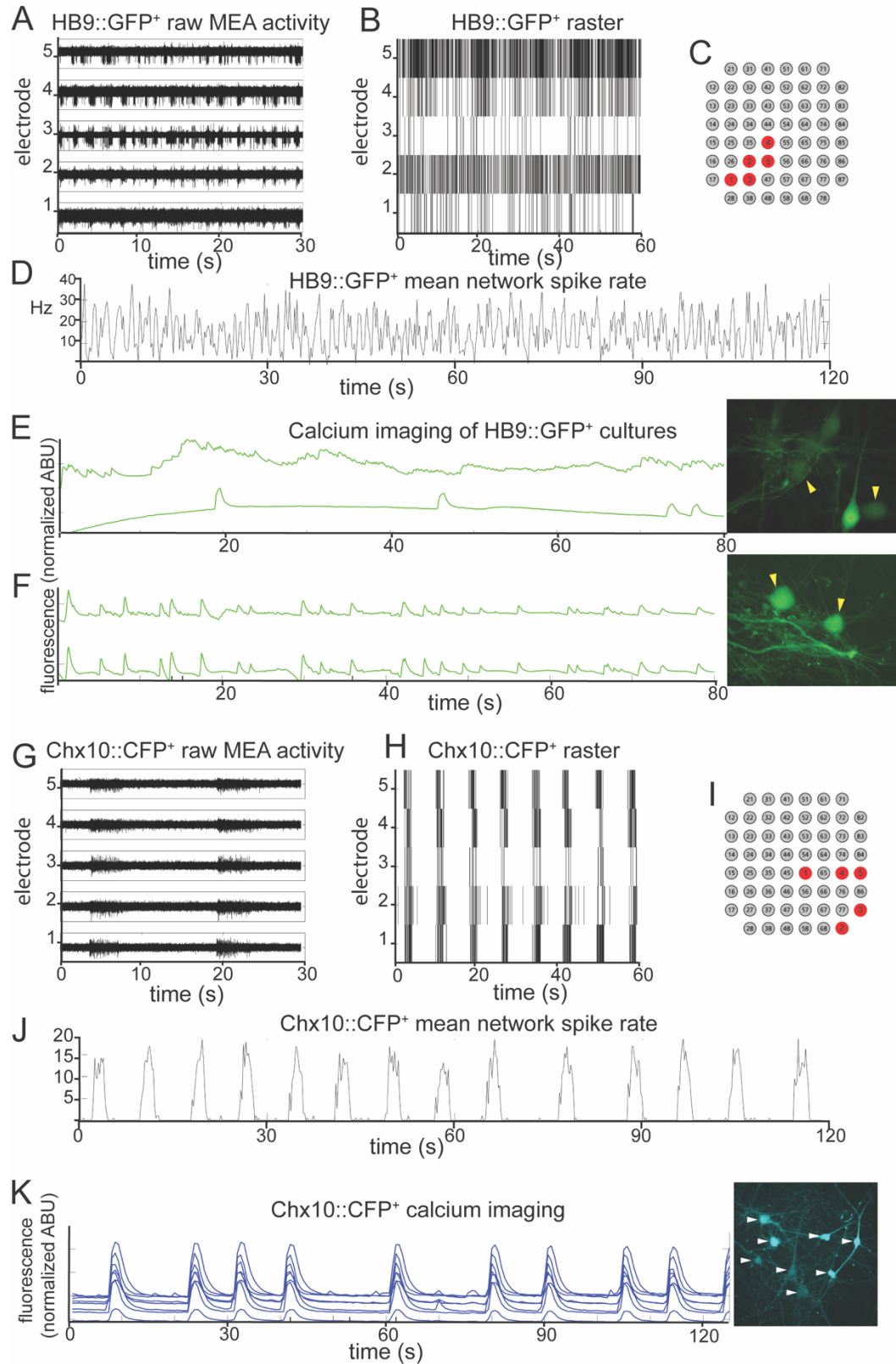
Figure 3

420

Figure 3

421

22

Figure 3: HB9$^+$ motor neurons and Chx10$^+$ hindbrain neurons develop different patterns of activity *in vitro*. **A-C** Example of a multielectrode array (MEA) recording of sorted HB9::GFP$^+$ neurons (18 DIC), both as **A**, high pass filtered MEA data and **B**, raster plot. Locations of electrodes indicated in red in **C**. **D**, Mean spike rate of entire HB9::GFP$^+$ neuron culture from A,B.

E-F Quantification of calcium-sensitive Rhodamine3 dye fluorescence in the cell bodies of HB9::GFP$^+$ neurons **E**, 19 DIC, see video 3-2 for rhodamine fluorescence time course, **F**, 32 DIC, see video 3-3. Corresponding right panels are photomicrographs of neurons quantified for calcium activity, indicated by yellow arrowheads.

G-I Example of a multielectrode array (MEA) recording of sorted Chx10::CFP$^+$ neurons (5 DIC) as **G**, high-pass filtered MEA data and **H**, raster plot. locations of electrodes on array in red in **I**.

J, Mean spike rate of entire Chx10::CFP$^+$ neuron culture from B,E. **K**, Calcium imaging of Chx10::CFP$^+$ neurons (10 DIC), also shown in video 3-4. Right panel is a photomicrograph of identified neurons quantified for calcium activity, indicated by white arrowheads.

422

423   When we cultured Chx10$^+$ hindbrain neurons on MEAs with a confluent layer of

424 astrocytes, we observed the emergence of spontaneous activity with these neurons as well.

425 Unlike HB9$^+$ neurons, Chx10$^+$ neurons developed robust and coordinated network bursts

426 (**Figure 3g-j**). Practically no spikes occurred outside of these sharply delineated bursting

427 periods. The time between bursts (inter-burst interval) varied between 2 and 10 seconds

428 throughout the lifetime of the cultures, with no apparent long-term trend. We observed the

429 same sort of robust network bursts in Chx10$^+$ hindbrain neuron cultures with calcium imaging

430 (**Figure 3k, Video 3-4**).

431 *Chx10$^+$ neurons impose their activity patterns on HB9$^+$ neurons in coculture*

432   Despite their common glutamatergic identity, we observed that HB9$^+$ and Chx10$^+$

433 hindbrain neurons develop distinct patterns of spontaneous network activity. If these two cell

434 types fail to form functional connections to one another *in vitro*, these patterns of activity

435 should remain unchanged in coculture, but if a unidirectional functional connection forms

436 between Chx10$^+$ and HB9$^+$ neurons, we might expect to see one activity pattern dominate in

437 coculture. To test these possibilities, we cultured the two cell types together as a mixed

438 population on MEAs and recorded their spontaneous activity daily over 30 days.
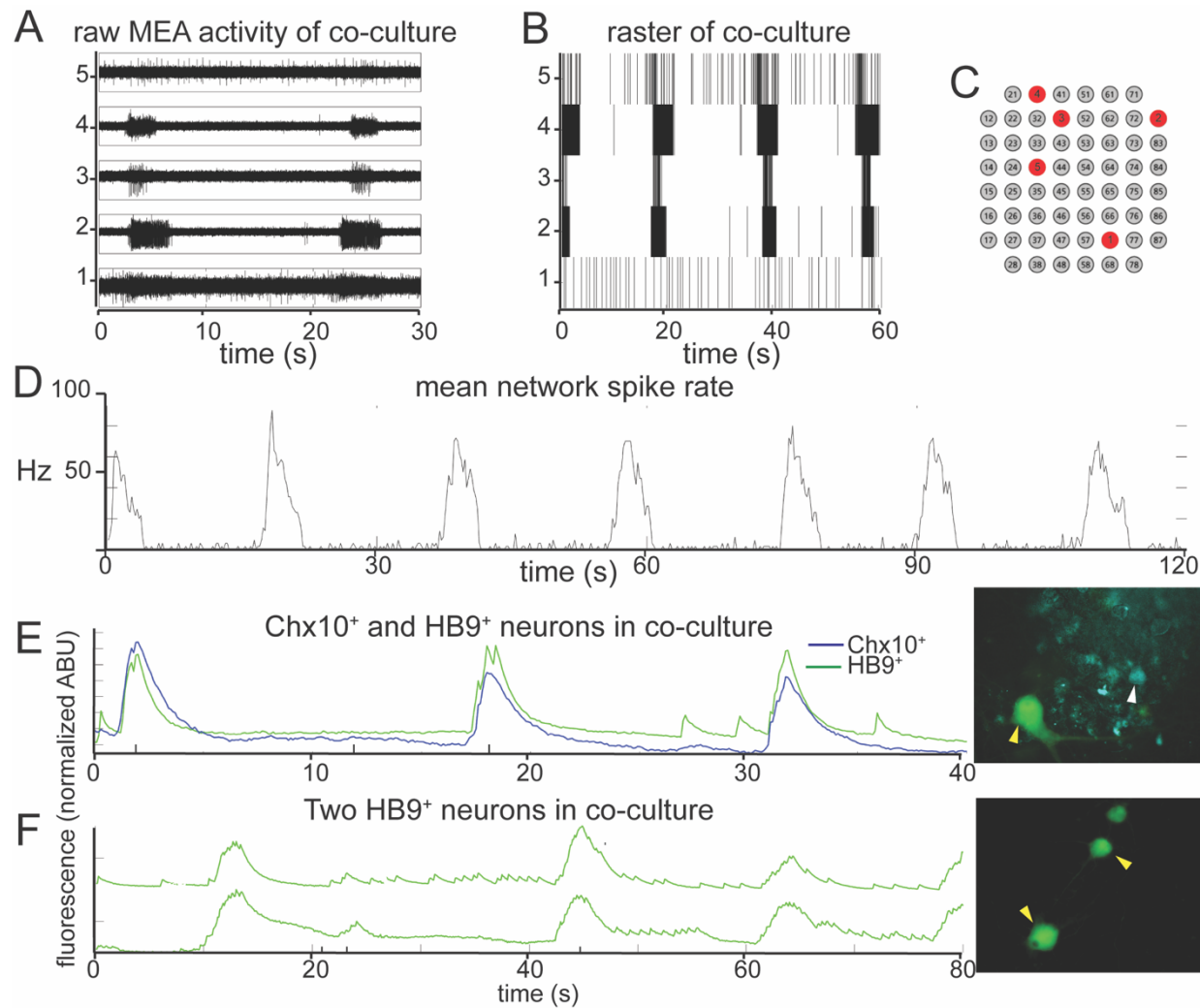
23

439

440

Figure 4: In reticulospinal co-culture, Chx10+ hindbrain neurons drive patterned HB9+ neuron activity. **A-B** Example of an MEA recording of HB9::GFP+/Chx10::CFP+ neuron coculture (8 DIC), both as **A**, high pass filtered MEA data and **B**, raster plot. Locations of electrodes indicated in red in **C**. **D**, Mean spike rate of entire co-culture from A, B over the course of 120 seconds.

E-F Calcium imaging of neurons in co-culture. **E**, Normalized calcium-sensitive fluorescence intensity over time in co-cultured HB9::GFP+ and Chx10::CFP+ neurons participating in coordinated bursts, shown also in video 4-1. **F**, Normalized calcium-sensitive fluorescence intensity of two HB9::GFP+ neurons from co-culture (Chx10::CFP+ neurons not pictured) participating in network bursts, shown also in video 4-2. Corresponding right panels indicate identified neurons quantified for calcium activity, white arrowheads for Chx10::CFP+ and yellow arrowheads for HB9::GFP+.

24

441 Such cocultures develop spontaneous bursts of comparable time scale and duration to pure

442 Chx10$^+$ cultures, though some neurons continue to have spiking activity that resembles HB9$^+$

443 motor neurons in between network bursts (**Figure 4a-c**). When the overall network activity was

444 measured by averaging spike rates across all active electrodes, the Chx10-like network bursts

445 predominated (**Figure 4d**).

446 It is possible that the bursts we observed in the reticulospinal culture were generated

447 only by the Chx10$^+$ neurons in the dish and that the HB9$^+$ motor neurons were quiescent and

448 did not contribute to network activity. In order to determine which cell type participates in the

449 cultures' network bursts, we used calcium imaging to obtain single cell resolution recordings of

450 the coculture. We found that neighboring HB9$^+$ and Chx10$^+$ neurons both participate in network

451 burst events (**Figure 4e, Video 4-1**). Some HB9$^+$ motor neurons in coculture also have brief,

452 non-coordinated calcium spiking events that occur between the larger bursts (**Figure 4f, Video**

453 **4-2**).

454 The percentages of Chx10$^+$ and HB9$^+$ neurons from calcium-imaging experiments that

455 were spiking, bursting, both spiking and bursting, or inactive in each of the culture conditions

456 are summarized in **Table 1**.

Cell type	Number total cells recorded	Spiking: number (percentage)	Bursting: number (percentage)	Spiking and Bursting: number (percentage)	No activity: number (percentage)
Chx10$^+$ (co-culture)	125	16 (13%)	64 (51%)	17 (14%)	28 (22%)
Chx10$^+$ (alone)	483	0	312 (65%)	7 (1%)	164 (34%)
HB9$^+$ (co-culture)	67	13 (19.5%)	13 (19.5%)	29 (43%)	12 (18%)
HB9$^+$ (alone)	176	81 (46%)	0	2 (1%)	93 (53%)

Table 1: Overview of activity patterns of Chx10$^+$ and HB9$^+$ neurons from calcium imaging experiments.

457

458

25

459   *HB9$^+$ and Chx10 network activity is an AMPA receptor-dependent process*

460   The spontaneous coordinated activity we observed in Chx10$^+$ and HB9$^+$ neuron cultures

461   could be the product of intrinsic pacemaker properties of these neurons or an emergent

462   property of the network that is dependent on synaptic transmission. To distinguish between

463   these alternatives, we applied a panel of synaptic blockers targeting α-amino-3-hydroxy-5-

464   methyl-4-isoxazolepropionic acid (AMPA) receptors, *N*-methyl D-aspartate (NMDA) receptors,

465   and γ-aminobutyric acid, type A (GABA$_A$) receptors, while recording from the cultures on MEAs

466   to observe changes in spontaneous activity. The blockers used included the AMPA receptor

467   antagonist 6-cyano-7-nitroquinoxaline-2,3-dione disodium salt (CNQX), the NMDA receptor

468   antagonist D-(-)-2-amino-5-phosphonopentanoic acid (AP5), and the GABA$_A$ receptor antagonist

469   bicuculline. Washing in the AMPA$_R$ antagonist CNQX on cultures of spiking HB9$^+$ neurons caused

470   a gradual decrease in activity to about 40% of initial levels (**Figure 5a, e**). There was a significant

471   relationship between drug dose and spike rates (linear mixed effects model: β = -0.04, p =

472   2.65e-63). Similarly, CNQX application resulted in a significant decrease in the activity of Chx10$^+$

473   neurons to about 40% of the initial rate (**Figure 5b, f**) (β = -0.021, p = 8.61e-15). The application

474   of CNQX to cocultures caused the majority of cells to abruptly stop bursting (**Figure 5c**). Other

475   neurons gradually became decoupled from the network bursts and fired tonically for a brief

476   period before also being silenced during CNQX application (figure 5d). The average response of

477   cocultured neurons to CNQX application reflects this transient increase in activity followed by

478   eventual inhibition (**Figure 5g**) (β = -0.012, p = 0.0015).

479

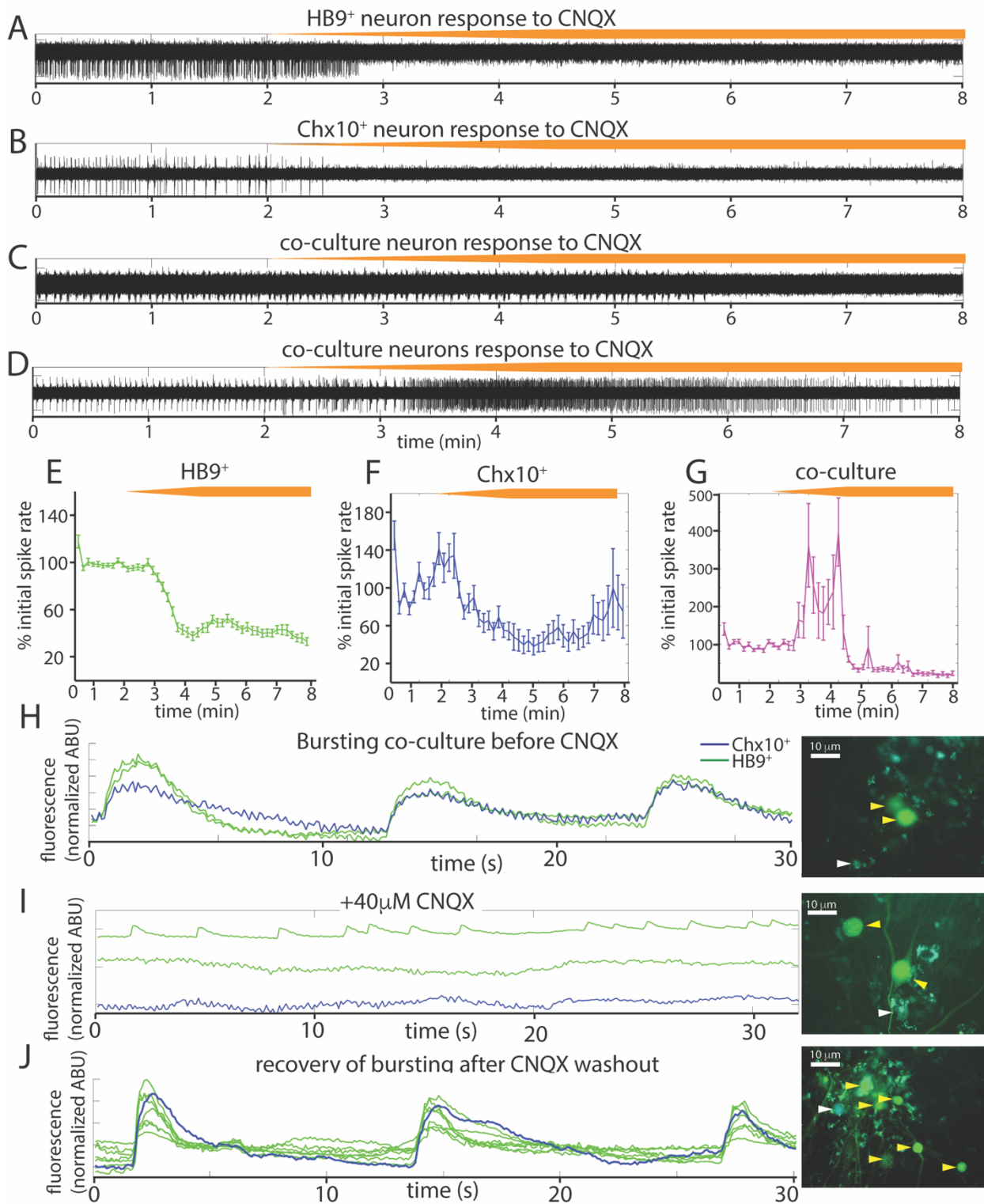**Figure 5**

480

481

482

27

Figure 5: Spontaneous activity in reticulospinal cultures is an AMPA$_R$-dependent process. **A-D**, Examples of high pass filtered MEA recordings of spiking neurons during wash-in of a 200μM solution of the AMPA$_R$ blocker CNQX at 50μL/min (final CNQX concentration 20μM), orange bars show time course of blocker wash-in. **A**, Neuron from HB9::GFP$^+$ culture, **B** neuron from Chx10::CFP$^+$ culture, **C-D** examples of two different kinds of responses to CNQX of neurons from HB9::GFP$^+$/Chx10::CFP$^+$ co-culture.
E-G, Normalized mean responses of all neurons recorded from electrodes with activity to CNQX wash-in, **E** HB9::GFP$^+$ cultures (n = 3), **F** Chx10::CFP$^+$ cultures (n = 3), **G** HB9::GFP$^+$/Chx10::CFP$^+$ co-cultures (n = 4).
H-J, Calcium imaging of co-culture **H**, bursting prior to CNQX application (shown also in video 5-1), **I**, inhibition of bursting, but not Hb9::GFP$^+$ spiking, by application of 40 μM CNQX (shown also in video 5-2), and **J**, bursting recovers after washout of CNQX (shown also in video 5-3). Corresponding right panels are photomicrographs of neurons quantified for calcium activity, indicated by white arrowheads for Chx10::CFP$^+$ and yellow arrowheads for HB9::GFP$^+$.

483

484   We repeated the CNQX drug application on cocultures and used calcium imaging with

485   Rhodamine3 to visualize the activity of the culture prior to and after application of 40μM CNQX.

486   Despite a loss of network bursting activity, we observed that some HB9$^+$ neurons in the

487   coculture continued to have spontaneous spiking activity in the presence of a blocking

488   concentration of CNQX (**Figure 5h-j**).

489   We also tested the effects of the NMDA receptor antagonist AP5 on all three cultures

490   (**Figure 6a-f**) and found that there was no significant relationship between blocker dose and

491   spike rates during AP5 wash-in (linear mixed effects model for: HB9$^+$ neurons, β = 0.0005 p =

492   0.23, Chx10$^+$ neurons, β = 0.004 p = 0.25, coculture, β = 0.006 p = 0.24). The GABA$_A$ receptor

493   blocker bicuculline also had no detectable effect on Chx10$^+$ hindbrain neurons, HB9$^+$ motor

494   neurons, or cocultures (**Figure 6g-l**) (linear mixed effects model for: HB9$^+$ neurons, β = 0.0003 p

495   = 0.54, Chx10$^+$ neurons, β = 0.0026 p = 0.34, coculture,β = 0.0057 p = 0.13).

28

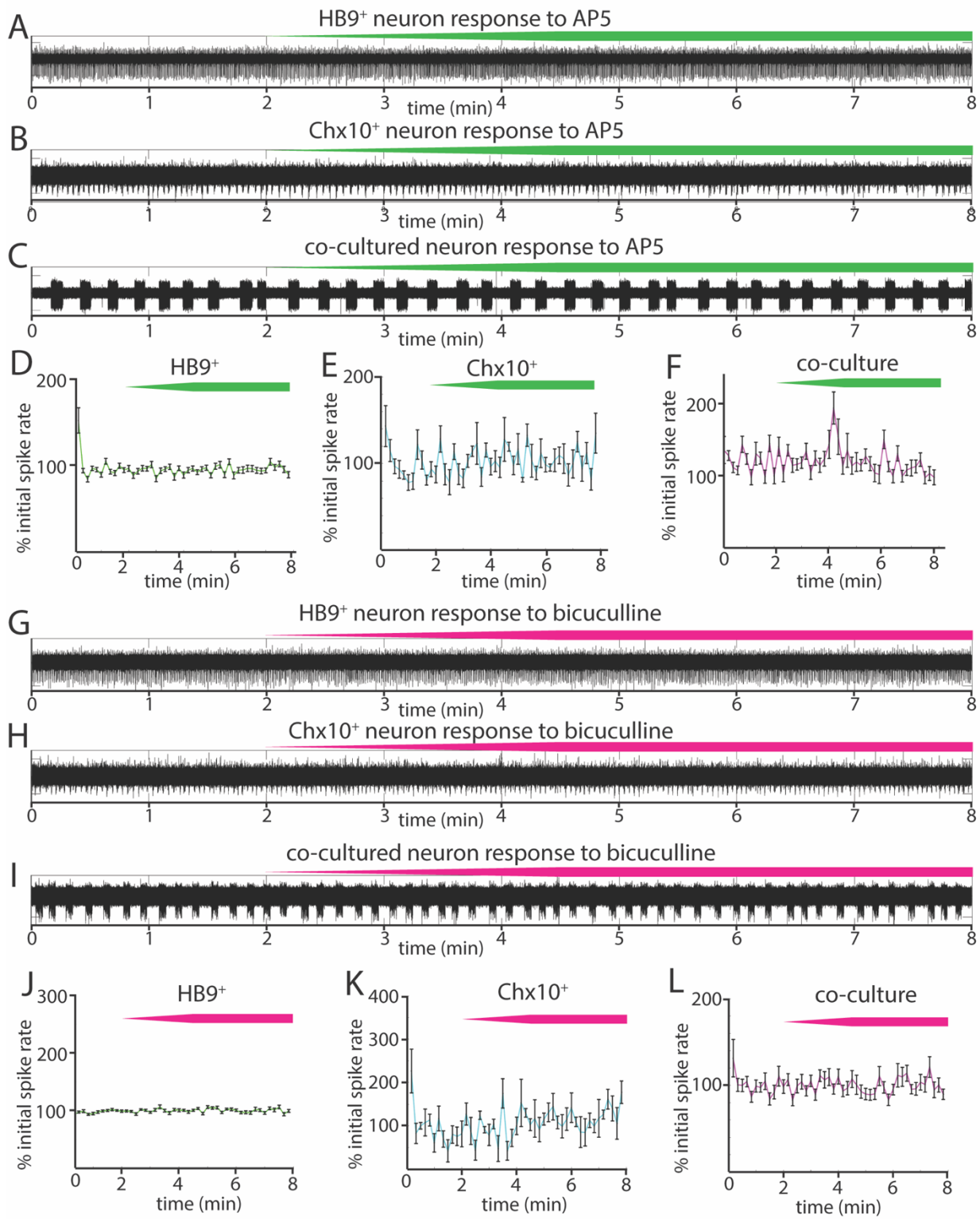**Figure 6**

496

497

29

Figure 6: Responses of reticulospinal cultures to $NMDA_R$ and $GABA_AR$ blockers. **A-C** Examples of high pass filtered MEA recordings of spiking neurons during wash-in of a 500μM solution of $NMDA_R$ blocker AP5 at 50μL/min (final AP5 concentration 50μM), green bars show approximate time course of AP5 wash-in. **A**, Neuron from HB9::GFP⁺ culture, **B** neuron from Chx10::CFP⁺ culture, **C** neuron from HB9::GFP⁺/Chx10::CFP⁺ coculture.

D-F, Normalized mean responses of all recorded neurons to AP5 wash-in, **D** HB9::GFP⁺ cultures (n = 3), **E** Chx10::CFP⁺ cultures (n = 3), **F** HB9::GFP⁺/Chx10::CFP⁺ co-cultures (n = 4).

G-I Examples of high pass filtered MEA recordings of spiking neurons during wash-in of a 600μM solution of $GABA_AR$ blocker bicuculline at 50μL/min (final bicuculline concentration 60μM), magenta bars show time course of bicuculline wash-in. **G**, Neuron from HB9::GFP⁺ culture, **H** neuron from Chx10::CFP⁺ culture, **I** neuron from HB9::GFP⁺/Chx10::CFP⁺ coculture.

J-L Normalized mean responses of all recorded neurons to bicuculline wash-in, **J** HB9::GFP⁺ cultures (n = 3), **K** Chx10::CFP⁺ cultures (n = 3), **L** HB9::GFP⁺/Chx10::CFP⁺ cocultures (n = 4).

498

499 **Discussion:**

500   In this study, we used flow cytometry to isolate HB9⁺ motor neurons and Chx10⁺

501 hindbrain neurons and cultured these cell types separately and together to form a

502 reticulospinal circuit. We found that the sorting process did not significantly impact the

503 development of HB9⁺ and Chx10⁺ neuron electrophysiology. When isolated, these two cell

504 types developed distinct patterns of network activity. HB9⁺ neurons tended towards

505 uncoordinated spike trains, while Chx10⁺ hindbrain neurons were characterized by regular,

506 network-wide bursts of activity. Cocultures of these two cell types developed the network

507 bursts characteristic of Chx10⁺ neurons that recruited neighboring HB9⁺ neurons. We further

508 note that the activity of all these cultures was insensitive to NMDA and $GABA_A$ receptor

509 blockers but could be inhibited by the AMPA receptor blocker CNQX.

510 *Effect of cell sorting on electrophysiology of isolated cells*

511   FACS-sorted stem-cell derived HB9⁺ motor neurons develop complex morphology and

512 electrical excitability *in vitro* (Uzel 2016, Yang 2013, Haidet-Phillips 2011, Wichterle 2002), but

513 previous studies had not established whether the nature of their electrical responses had been

514 altered. Our results show that sorted Hb9⁺ motor neurons develop spontaneous spiking activity,

30

515   fast inactivating sodium currents, and repetitive trains of action potentials in response to

516   current injection. These results are consistent with the reported electrophysiology of unsorted

517   stem cell-derived motor neurons (Miles 2004). Thus, our single-cell electrophysiology indicates

518   that the presence of other neuronal subtypes and progenitors does not alter the electrical

519   properties of HB9^{+} motor neurons, indicating that they are determined by cell type identity.

520   We found that FACS-sorted Chx10^{+} hindbrain neurons developed spontaneous rhythmic

521   bursting activity *in vitro*. While there are no *in vitro* studies on unsorted hindbrain Chx10^{+}

522   neurons, this behavior is consistent with the observation that a closely related population of

523   spinal V2a neurons develops spontaneous rhythmic activity following FACS isolation and

524   reaggregation into three-dimensional cultures (Sternfeld 2017). Thus, FACS is a viable option for

525   the isolation and subsequent long-term culture of molecularly defined neuronal subtypes.

526   *Cell type specific patterns of activity in cultures of sorted neurons*

527   Several prior studies have arranged neurons on MEAs in very specific patterns (Maher

528   1999, Wheeler 2010), but not defined subtypes. The random patterning of molecularly defined

529   cells on our arrays allowed us to explore whether there is a consistent influence of cell type on

530   network behavior, regardless of network architecture.

531   Our observation that HB9^{+} motor neurons fail to develop spontaneous activity in the

532   absence of glia is consistent with other studies that have demonstrated the essential support

533   that astrocytes provide for cultured neurons (Wang 1994, Boehler 2007), including motor

534   neurons (Ullian 2004). When we cultured sorted HB9^{+} neurons with astrocytes they developed

535   unsynchronized spike trains. FACS appears to be critical for this behavior, as previous studies of

536   stem cell-derived HB9^{+} motor neurons cultured without FACS isolation reported coordinated

31

537   network bursts (Jenkinson 2017). In unsorted cultures, a cell type other than HB9$^+$ neurons

538   must have contributed to the generation of this activity pattern. We note that the spinal motor

539   neuron differentiation protocol generates a small but prominent subpopulation of spinal V2a

540   neurons, a cell type that is closely related to our rhythmogenic hindbrain Chx10$^+$ neurons

541   (Brown 2014).

542   We found that Chx10$^+$ hindbrain neurons isolated by FACS and cultured on MEAs

543   developed robust and highly coordinated network bursts. Calcium imaging (**Figure 3**) indicates

544   that virtually all Chx10$^+$ neurons participate in these bursts, with no discernible time delay.

545   Thus, simultaneous spiking is an intrinsic feature of Chx10$^+$ neurons in culture and does not

546   appear to require the presence of other cell types.

547   *Chx10-like pattern of activity is dominant in coculture*

548   Recordings from the coculture indicate that Chx10$^+$ neurons impose their rhythmic

549   bursting phenotype on adjacent HB9$^+$ neurons (**Figure 4e**). In this way, we were able to induce

550   HB9$^+$ neurons to participate in network bursts by exposing them to another rhythmogenic cell

551   type. Purified cultured HB9$^+$ neurons did not coordinate their spontaneous calcium spikes

552   despite being adjacent to each other. Thus, HB9$^+$ neurons appear to require patterned input

553   from another cell type. In contrast, Chx10$^+$ hindbrain neurons are able to generate their own

554   patterns of activity without the need for exogenous cell types besides astrocytes. In summary,

555   our results indicate that when cultured with astrocytes, electrically excitable cell types develop

556   different spontaneous patterns of activity that are driven by the intrinsic properties of that cell

557   type.

558   We were unable to detect any spontaneous activity in cultures without astrocytes,

559   consistent with previous results with neuronal culture on MEAs (Ullian 2004, Boehler 2007). It is

560   likely that one way that astrocytes mediate such an effect is by removing excess glutamate to

561   prevent excitotoxicity (Rothstein 1996, Swanson 1997). Consistent with previous reports

562   (Scemes 2006), the astrocytes in our culture were active, as indicated by slow waves of calcium

563   activity which we were able to observe in calcium imaging (**Video 3-1**), but which did not

564   produce electrical excitation on MEAs.

565   Our observation that Chx10$^+$ neurons are able to impose temporally patterned activity

566   on HB9$^+$ neurons is consistent with their *in vivo* function of driving rhythmic behaviors such as

567   hindlimb locomotion and respiration. Prior studies suggest that activation of these neurons is

568   associated with bouts of locomotion, and may drive locomotor stop signals (Bretzner, 2013,

569   Bouvier 2015). Additionally, Chx10$^+$ neurons project to the pre-Bötzinger complex, and their

570   ablation disrupts respiratory rhythms in newborn mice, with normal respiratory rhythms

571   gradually reasserting themselves as the mice grow older (Crone 2012, Crone 2009).

572   *Emergent properties of neuronal cultures as revealed by synaptic inhibition*

573   Our results from applying a panel of synaptic blockers targeting AMPA, NMDA, and

574   GABA$_A$ receptors to spontaneously active HB9$^+$ and Chx10$^+$ neuron cultures (**Figures 5 and 6**)

575   show that the AMPA$_R$ blocker CNQX effectively blocked all bursts in Chx10$^+$ cultures and

576   significantly decreased the activity in HB9$^+$ neuron cultures. This is consistent with the

577   observation that spinal motor neurons cultured *in vitro* form glutamatergic synapses that are

578   entirely blocked by CNQX (Ullian 2004). CNQX application similarly eradicates spontaneous

579   network bursting in cultures of spinal Chx10$^+$ neurons that are otherwise insensitive to glycine

580   and GABA antagonists (Sternfeld 2017). Our finding that bursts of hindbrain Chx10⁺ neurons

581   could be effectively eradicated by blocking glutamatergic transmission suggests that the robust

582   rhythmicity of these neurons is an emergent property of the network, as opposed to pacemaker

583   activity generated by individual cells. This contrasts with true pacemaker neurons, such as

584   those of the pre-Bötzinger complex, where bursts are intrinsic to individual cells, and therefore

585   insensitive to the same cocktail of synaptic blockers (Chevalier 2016). Thus, we observe that

586   AMPA receptor activation can drive very different outcomes that depend on cell type.

587   When we applied CNQX to the coculture, some neurons switched from rhythmic

588   bursting to a transient period of tonic spiking before becoming quiescent. This emergent

589   property may be driven by HB9⁺ neurons that revert to their native spiking phenotype in the

590   absence of the patterning influence of network bursts. This is consistent with our calcium

591   imaging data in which we identified HB9⁺ neurons in coculture that continued to have calcium

592   spikes even in the presence of a dose of CNQX that effectively disrupted network bursts (**Figure**

593   **5**).

594   *Implications of our results for modeling reticulospinal circuits*

595   The results of our study could be applied to modeling of reticulospinal circuits, different

596   aspects of which are currently being examined by multiple groups (Sternfeld 2017, Oueghlani

597   2018, Pivetta 2014). In the rodent reticulospinal circuit, hindbrain Chx10⁺ neurons primarily

598   contact premotor networks within the spinal cord, as opposed to synapsing directly onto motor

599   neurons (Bouvier 2015). By contrast, in the zebrafish hindbrain Chx10⁺ neurons directly contact

600   spinal motor neurons and generate swimming when selectively stimulated (Kimura 2013).

601   Likewise, in *Xenopus* tadpoles the Chx10⁺ dorsoventral hindbrain provides patterned excitatory

602   input directly to motor neurons, driving sensory-evoked swimming before other motor control

603   systems have developed (Soffe 2009, Li 2019). Thus, it can be argued that the circuit created by

604   our *in vitro* cocultures replicates the basic circuitry found in fish and amphibians. It would be

605   interesting to determine whether the emergent properties of Chx10$^+$ neurons from these

606   species differ from the mouse, and how incorporating additional reticulospinal cell types would

607   alter patterns of activity.

608   Ultimately, the most generalizable aspect of the findings we report here is the

609   observation that the aggregate activity of neuronal networks is influenced by the specific

610   molecular identity of their constituent neurons, beyond specific pacemaker cells or broad

611   categories of excitatory-inhibitory cells. Our results indicate that many electrical properties of

612   neurons are intrinsic to their specific subtype, which is an important consideration for modeling

613   the effects of mutations and disease on network function. The cell type compositions of circuit

614   models can have profound effects on patterns of activity and need to be considered and

615   interpreted carefully.

35

632   **References:**

633   Binder MD, Heckman CJ, Powers RK (1996) The physiological control of motoneuron activity.

634   In: Handbook of Physiology, pp 3–53.

635   Black BJ, Atmaramani R, Pancrazio JJ (2017) Spontaneous and Evoked Activity from Murine

636   Ventral Horn Cultures on Microelectrode Arrays. Front Cell Neurosci 11.

637   Boehler MD, Wheeler BC, Brewer GJ (2007) Added astroglia promote greater synapse density

638   and higher activity in neuronal networks. Neuron Glia Biol 3:127–140.

639   Bouvier J, Caggiano V, Leiras R, Caldeira V, Bellardita C, Balueva K, Fuchs A, Kiehn O (2015)

640   Descending Command Neurons in the Brainstem that Halt Locomotion. Cell 163:1191–

641   1203.

642   Bretzner F, Brownstone RM (2013) Lhx3-Chx10 reticulospinal neurons in locomotor circuits. J

643   Neurosci 33:14681–14692.

644   Brown CR, Butts JC, McCreedy DA, Sakiyama-Elbert SE (2014) Generation of V2a

645   Interneurons from Mouse Embryonic Stem Cells. Stem Cells Dev 23:1765–1776.

646   Chevalier M, Toporikova N, Simmers J, Thoby-Brisson M (2016) Development of pacemaker

647   properties and rhythmogenic mechanisms in the mouse embryonic respiratory network.

648   Elife 5.

649   Chiappalone M, Bove M, Vato A, Tedesco M, Martinoia S (2006) Dissociated cortical networks

650   show spontaneously correlated activity patterns during in vitro development. Brain Res

651   1093:41–53.

652   Crone SA, Viemari J-C, Droho S, Mrejeru A, Ramirez J-M, Sharma K (2012) Irregular

653   Breathing in Mice following Genetic Ablation of V2a Neurons. J Neurosci 32:7895–7906.

654   Crone SA, Zhong G, Harris-warrick R, Sharma K (2009) In Mice Lacking V2a Interneurons ,

655   Gait Depends on Speed of Locomotion. J Neurosci 29:7098–7109.

656   Dauth S, Maoz BM, Sheehy SP, Hemphill MA, Murty T, Macedonia MK, Greer AM, Budnik B,

657   Parker KK (2016) Neurons derived from different brain regions are inherently different in

658   vitro: A novel multiregional brain-on-a-chip. J Neurophysiol 117:1320–1341.

659   Fantin A, Vieira JM, Plein A, Maden CH, Ruhrberg C (2013) The embryonic mouse hindbrain as

660   a qualitative and quantitative model for studying the molecular and cellular mechanisms of

661   angiogenesis. Nat Protoc 8:418–429.

662   Garcia-Rill E, Skinner RD (1987a) The mesencephalic locomotor region. I. Activation of a

663   medullary projection site. Brain Res 411:1–12.

664   Garcia-Rill E, Skinner RD (1987b) The mesencephalic locomotor region. II. Projections to

665   reticulospinal neurons. Brain Res 411:13–20.

666   Haidet-Phillips AM, Hester ME, Miranda CJ, Meyer K, Braun L, Frakes A, Song S, Likhite S,

667   Murtha MJ, Foust KD, Rao M, Eagle A, Kammesheidt A, Christensen A, Mendell JR,

668   Burghes AHM, Kaspar BK (2011) Astrocytes from familial and sporadic ALS patients are

669   toxic to motor neurons. Nat Biotechnol 29:824–828.

670   Jenkinson SP, Grandgirard D, Heidemann M, Tscherter A, Avondet M, Leib SL (2017)

671   Embryonic Stem Cell-Derived Neurons Grown on Multi-Electrode Arrays as a Novel In

672   vitro Bioassay for the Detection of Clostridium botulinum Neurotoxins. Front Pharmacol 8.

673   Kiehn O (2016) Decoding the organization of spinal circuits that control locomotion. Nat Publ

674   Gr 17:224–238.

675   Kimura Y, Satou C, Fujioka S, Shoji W, Umeda K, Ishizuka T, Yawo H, Higashijima SI (2013)

676   Hindbrain V2a neurons in the excitation of spinal locomotor circuits during zebrafish

677   swimming. Curr Biol 23:843–849.

678   Le Ray D, Juvin L, Ryczko D, Dubuc R (2011) Supraspinal control of locomotion: The

679   mesencephalic locomotor region. Prog Brain Res 188:51-70.

680   Li W-C, Soffe SR (2019) Stimulation of Single, Possible CHX10 Hindbrain Neurons Turns

681   Swimming On and Off in Young Xenopus Tadpoles. Front Cell Neurosci 13.

682   Li X, Sun J, Chen W, Zeng S, Luo Q (2009) The generation of the synchronized burst in cultured

683   neuronal networks. Proc SPIE, Int Soc Opt Eng 7176.

684   Lonardoni D, Amin H, Di Marco S, Maccione A, Berdondini L, Nieus T (2017) Recurrently

685   connected and localized neuronal communities initiate coordinated spontaneous activity in

686   neuronal networks. PLoS Comput Biol 13.

687   Maher MP, Dvorak-Carbone H, Pine J, Wright JA, Tai Y-C (1999) Microstructures for studies of

688   cultured neural networks. Med Biol Eng Comput 37:110–118.

689   Maheswaranathan N, Ferrari S, VanDongen A, Henriquez C (2012) Emergent bursting and

690   synchrony in computer simulations of neuronal cultures. Front Comput Neurosci 6:1–11.

691   Oueghlani Z, Simonnet C, Cardoit L, Courtand G, Cazalets J-R, Morin D, Juvin L, Barrière G

692   (2018) Brainstem steering of locomotor activity in the newborn rat. J Neurosci 38:7725–

693   7740.

694   Peterson B (1979) Reticulospinal Projections to Spinal Motor Nuclei. Annu Rev Physiol 41:127–

695   140.

696   Pivetta C, Esposito MS, Sigrist M, Arber S (2014) Motor-circuit communication matrix from

697   spinal cord to brainstem neurons revealed by developmental origin. Cell 156:537–548.

698   Rothstein JD, Dykes-Hoberg M, Pardo CA, Bristol LA, Jin L, Kuncl RW, Kanai Y, Hediger

699   MA, Wang Y, Schielke JP, Welty DF (1996) Knockout of Glutamate Transporters Reveals

700   a Major Role for Astroglial Transport in Excitotoxicity and Clearance of Glutamate. Neuron

701   16:675–686.

702   Sarkar A, Mei A, Paquola ACM, Stern S, Bardy C, Klug JR, Kim S, Neshat N, Kim HJ, Ku M,

703   Shokhirev MN, Adamowicz DH, Marchetto MC, Jappelli R, Erwin JA, Padmanabhan K,

704   Shtrahman M, Jin X, Gage FH (2018) Efficient Generation of CA3 Neurons from Human

705   Pluripotent Stem Cells Enables Modeling of Hippocampal Connectivity In Vitro. Cell Stem

706   Cell 22:684–697.

707   Scemes E, Giaume C (2006) Astrocyte Calcium Waves: What They Are and What They Do.

708   Glia 54:716–725.

709   Schildge S, Bohrer C, Beck K, Schachtrup C (2013) Isolation and Culture of Mouse Cortical

710   Astrocytes. J Vis Exp:1–7.

711   Soffe SR, Roberts A, Li WC (2009) Defining the excitatory neurons that drive the locomotor

712   rhythm in a simple vertebrate: Insights into the origin of reticulospinal control. J Physiol

713   587:4829–4844.

714   Soscia D, Belle A, Fischer N, Enright H, Sales A, Osburn J, Benett W, Mukerjee E, Kulp K,

715   Pannu S, Wheeler E (2017) Controlled placement of multiple CNS cell populations to create

716   complex neuronal cultures. PLoS One 12.

717   Sternfeld MJ, Hinckley CA, Moore NJ, Pankratz MT, Hilde KL, Driscoll SP, Hayashi M, Amin

718   ND, Bonanomi D, Gifford WD, Sharma K, Goulding M, Pfaff SL (2017) Speed and

719   segmentation control mechanisms characterized in rhythmically-active circuits created from

720   spinal neurons produced from genetically-tagged embryonic stem cells. Elife 6.

721   Swanson RA, Liu J, Miller JW, Rothstein JD, Farrell K, Stein BA, Longuemare MC (1997)

722   Neuronal regulation of glutamate transporter subtype expression in astrocytes. J Neurosci

723   17:932–940.

724   Trujillo CA, Gao R, Negraes PD, Chaim IA, Domissy A, Vandenberghe M, Devour A, Yeo GW,

725   Voytek B, Muotri AR (2018) Nested oscillatory dynamics in cortical organoids model early

726   human brain network development. bioRxiv 358622.

727   Ullian EM, Harris BT, Wu A, Chan JR, Barres BA (2004) Schwann cells and astrocytes induce

728   synapse formation by spinal motor neurons in culture. Mol Cell Neurosci 25:241–251.

729   Uzel SGM, Platt RJ, Subramanian V, Pearl TM, Rowlands CJ, Chan V, Boyer LA, So PTC,

730   Kamm RD (2016) Microfluidic device for the formation of optically motor units. Sci Adv 2.

731   Van Pelt J, Vajda I, Wolters PS, Corner MA, Ramakers GJA (2005) Dynamics and plasticity in

732   developing neuronal networks in vitro. Prog Brain Res 147:173–188.

733   Wagenaar DA, Pine J, Potter SM (2006) An extremely rich repertoire of bursting patterns during

734   the development of cortical cultures. BMC Neurosci 7.

735   Wainger BJ, Buttermore ED, Oliveira JT, Mellin C, Lee S, Saber WA, Wang AJ, Ichida JK,

736   Chiu IM, Barrett L, Huebner EA, Bilgin C, Tsujimoto N, Brenneis C, Kapur K, Rubin LL,

737   Eggan K, Woolf CJ (2015) Modeling pain in vitro using nociceptor neurons reprogrammed

738   from fibroblasts. Nat Neurosci 18:17–24 Available at: http://dx.doi.org/10.1038/nn.3886.

739   Wang LC, Baird DH, Hatten ME, Mason CA (1994) Astroglial differentiation is required for

740   support of neurite outgrowth. J Neurosci 14:3195–3207.

741 Wheeler BC, Brewer GJ (2010) Desingning neural networks in culture. Proc IEEE 98:398–406.

742 Wichterle H, Lieberam I, Porter JA, Jessell TM (2002) Directed differentiation of embryonic

743   stem cells into motor neurons. Cell 110:385–397.

744 Yang YM, Gupta SK, Kim KJ, Powers BE, Cerqueira A, Wainger BJ, Ngo HD, Rosowski KA,

745   Schein PA, Ackeifi CA, Arvanites AC, Davidow LS, Woolf CJ, Rubin LL (2013) A Small

746   Molecule Screen in Stem-Cell-Derived Motor Neurons Identifies a Kinase Inhibitor as a

747   Candidate Therapeutic for ALS. Cell Stem Cell 12:713–726.

748 Zhong G, Droho S, Crone SA, Dietz S, Kwan AC, Webb WW, Sharma K, Harris-warrick RM

749   (2010) Electrophysiological Characterization of V2a Interneurons and Their Locomotor-

750   Related Activity in the Neonatal Mouse Spinal Cord. J Neurosci 30:170–182.

751

752 **Supplemental data captions:**

753 **Video 3-1**: Calcium imaging of glia. Time course of Rhodamine3 fluorescence of astrocyte

754 culture with spontaneous calcium activity. Playback of time 1-130s from raw recording (total

755 time of raw recording is 130s). Minimum value of each pixel from the entire recording was

756 subtracted from that corresponding pixel in each frame to minimize noise.

757

758 **Video 3-2**: Calcium imaging of spiking HB9^{+} neurons. Time course of Rhodamine3 fluorescence

759 that corresponds to quantification in figure 3E. Playback of time 1-12s from raw recording (total

760 time of raw recording is 80s). ROIs used to quantify HB9^{+} neuron calcium activity are outlined in

761 yellow. Minimum value of each pixel from the entire recording was subtracted from that

762 corresponding pixel in each frame to minimize noise.

763

764   **Video 3-3**: Calcium imaging of HB9$^+$ neurons with coordinated spiking. Time course of

765   Rhodamine3 fluorescence that corresponds to quantification in figure 3F. Playback of time 1-

766   15s from raw recording (total time of raw recording is 80s). ROIs used to quantify GFP$^+$ neuron

767   calcium activity are outlined in yellow. Minimum value of each pixel from the entire recording

768   was subtracted from that corresponding pixel in each frame to minimize noise.

769

770   **Video 3-4**: Calcium imaging of Chx10$^+$ neuron network bursts. Time course of Rhodamine3

771   fluorescence that corresponds to quantification in figure 3K. Playback of time 1-130s from raw

772   recording. ROIs used to quantify Chx10$^+$ neuron calcium activity are outlined in yellow.

773

774   **Video 4-1**: Calcium imaging of HB9$^+$/Chx10$^+$ neuron coculture. Time course of Rhodamine3

775   fluorescence that corresponds to quantification in figure 4E. Playback of time 40-80s from raw

776   recording (total time of raw recording is 80s). ROI used to quantify HB9$^+$ neuron's calcium

777   activity is outlined in green, ROI used to quantify Chx10$^+$ neuron's calcium activity is outlined in

778   cyan. Minimum value of each pixel from the entire recording was subtracted from that

779   corresponding pixel in each frame to minimize noise.

780

781   **Video 4-2**: Calcium imaging of HB9$^+$ neurons in HB9$^+$/Chx10$^+$ neuron coculture. Time course of

782   Rhodamine3 fluorescence that corresponds to quantification in figure 4F. Playback of time 1-

783   80s from raw recording. ROIs used to quantify HB9$^+$ neuron calcium activity are outlined in

784   green. Minimum value of each pixel from the entire recording was subtracted from that

785   corresponding pixel in each frame to minimize noise.

786 **Video 5-1**: Calcium imaging of bursting HB9$^+$/Chx10$^+$ neuron coculture prior to AMPA$_R$ blocker

787 application. Time course of Rhodamine3 fluorescence that corresponds to quantification in

788 figure 5H. Playback of time 35-75s rom raw recording (total time of raw recording is 80s). ROIs

789 used to quantify HB9$^+$ neuron calcium activity are outlined in green, ROI used to quantify

790 Chx10$^+$ neuron's calcium activity is outlined in cyan. Minimum value of each pixel from the

791 entire recording was subtracted from that corresponding pixel in each frame to minimize noise.

792

793 **Video 5-2**: Calcium imaging of HB9$^+$ neurons in co-culture after application of 40μM AMPA$_R$

794 blocker. Time course of Rhodamine3 fluorescence that corresponds to quantification in figure

795 5I. Playback of time 8-38s from raw recording (total time of raw recording is 80s). ROIs used to

796 quantify HB9$^+$ neuron calcium activity are outlined in green, ROI used to quantify Chx10$^+$

797 neuron's calcium activity is outlined in cyan. Minimum value of each pixel from the entire

798 recording was subtracted from that corresponding pixel in each frame to minimize noise.

799

800 **Video 5-3**: Calcium imaging of bursting HB9$^+$/Chx10$^+$ neuron coculture after washout of AMPA$_R$

801 blocker. Time course of Rhodamine3 fluorescence that corresponds to quantification in figure

802 5J. Playback of time 10-40s from raw recording (total time of raw recording is 80s). ROIs used to

803 quantify HB9$^+$ neuron calcium activity are outlined in green, ROI used to quantify Chx10$^+$

804 neuron's calcium activity is outlined in cyan. Minimum value of each pixel from the entire

805 recording was subtracted from that corresponding pixel in each frame to minimize noise.